ORIGINAL ARTICLE

Relationships between spectral features, iron oxides and colours of surface soils in northern Jordan

Wahib Sahwan[1] | **Bernhard Lucke[1]** | **Tobias Sprafke[2]** | **Kim A. Vanselow[1]** | **Rupert Bäumler[1]**

[1]Institute of Geography, FAU Erlangen-Nürnberg, Erlangen, Germany

[2]Institute of Geography, University of Bern, Bern, Switzerland

Correspondence
Wahib Sahwan, Institute of Geography, FAU Erlangen-Nürnberg, Wetterkreuz 15, 91058 Erlangen, Germany.
Email: wahib.sahwan@fau.de

Abstract

Ground data on spectral characteristics of Jordan's soils remain sparse, which makes the interpretation of remote sensing datasets challenging. These are, however, very useful for predicting soil properties and agricultural suitability. Previous studies have shown that soil colours correlate well with degrees of weathering intensity, as indicated by magnetic parameters and dithionite-extractable iron (Fe_d) contents along a climosequence in northern Jordan. This study enlarges the database by the results of 160 bulk samples that were collected systematically from the soil surface at 40 locations. In addition to soil colour and contents of Fe_d, we explore mean soil reflectance spectra (MSRS) measured by analytical spectral devices (ASD) and analyse the morphological conditions of the spectra referring to the effects of iron oxides on spectral behaviours. Results show a high correlation of spectral behaviours and colour variations with Fe oxides, and no correlation with soil organic carbon C_{org}. The influence of the Fe oxide contents is clearly apparent in the visible range (VIS). The presence of $CaCO_3$ increases the reflectance in all spectral ranges. Six soil groups (Gr. I - Gr. VI) were discerned qualitatively and quantitatively in the study area, which largely mirror the intensity of red colour expressed by redness indices.

Highlights

- In northwestern Jordan there is an evident connection between the spectral properties, chemistry and soil colour.
- This study established a preliminary spectral library of soils in NW Jordan to facilitate the use of remote sensing in soil studies.
- The morphological properties and statistical analysis of the spectral data show that spectra of soils in NW Jordan are dominated by iron oxides.
- Spectral properties can be used to characterize the soil colours and types of Fe oxides in soils of Jordan.

1 | INTRODUCTION

The north-western part of Jordan is located in the Mediterranean climate zone. Soil cover is limited in extent and essential for agricultural production, as climatic conditions are not favourable for agriculture in most parts of Jordan. Sustainable soil management and development of the agricultural and pastoral land-use sectors are of major concern in the region and require knowledge on the spatial variations of soils and their properties. Apart from various case studies on soil development, erosion-sedimentation and land-use history of north-western Jordan (Lucke, 2008, 2017; Lucke et al., 2008; Lucke, Kemnitz, & Bäumler, 2012; Lucke, Kemnitz, Bäumler, & Schmidt, 2014; Lucke, Schmidt, Bens, & Hüttl, 2005; Schmidt et al., 2006), several soil classification and mapping campaigns were executed in the country to support soil management and land-use planning at the national level (see summary by Lucke, Ziadat, & Taimeh, 2013). The first significant work in this field started in 1950 and recognized 12 great soil groups at a scale of 1:1,000,000 (Moormann, 1959). The resulting report applied older versions of the US Soil Taxonomy (USDA, 1938), with special reference to soil colour. Another detailed soil survey in the 1970s was restricted to the regions around Irbid (NW Jordan) and Karak (W Jordan) (Al-Qudah, 2001). However, the only systematic, nationwide soil survey and land classification was conducted in 1989–1993, resulting in soil maps at three different levels of detail (NSM and LUP, 1993). The initial survey of this project was a reconnaissance study using the visual analysis of Landsat and aerial photography (Al-Qudah, 2001). Due to poor information on spectral characteristics of the soils, there was no possibility to seriously re-evaluate previous soil mappings or to support spatially oriented soil studies in Jordan with newly available remote sensing data. Consequently, there is a need for ground-based imaging spectroscopy to study soil spectral reflectance features, in order to understand their relation to soil properties and as a reference for the application of remote sensing in soil mapping of Jordan (Chabrillat et al., 2019; Huete, 1996; Viscarra Rossel et al., 2016).

The use of spectroscopy in soil studies started in the 1960s and 1970s (Bowers & Hanks, 1965). In comparison with human visual perception, which can only detect wavelengths from the visible range (VIS: 380 to 700 nm), spectroscopy has made it possible to extend that range into the near infrared (NIR: 700–1,100 nm) and shortwave infrared (SWIR: 1100–2,500 nm) ranges. The spectral range 350–2,500 nm is rich in information with regard to soil properties (Viscarra Rossel & Webster, 2011). As a result, the interest in the use of spectroscopy as a quick, inexpensive, reproducible and repeatable analytical technique for soil characterization and prediction of soil properties is growing (Nocita et al., 2015; Viscarra Rossel, Walvoort, McBratney, Janik, & Skjemstad, 2006). Furthermore, spectroscopy offers an alternative method for soil monitoring, surveying and land-use planning in combination with remote sensing data (Brown, Shepherd, Walsh, Dewayne Mays, & Reinsch, 2006; Chabrillat et al., 2019; Escadafal, Girard, & Courault, 1989; Hill & Schütt, 2000; Irons, Weismiller, & Peterson, 1989). These methods are currently undergoing further development for predictions of soil properties, and improved soil classifications using cluster-based statistical calculations (Ogen, Zaluda, Francos, Goldshleger, & Ben-Dor, 2019; Poppiel et al., 2018; Viscarra Rossel, Rizzo, Demattê, & Behrens, 2010). Several studies highlighted the relationships between the shapes and features of spectra and soil properties such as moisture, minerals, organic matter contents, colours, etc. (e.g., Baumgardner, Silva, Biehl, & Stoner, 1986; Huete & Escadafal, 1991; Stoner & Baumgardner, 1981). Other studies of this kind focused on retrieving information on soil colours and iron oxides as main chromophores (e.g., Ben-Dor, 2002; Camargo et al., 2015; Escadafal & Huete, 1992; Irons et al., 1989; Zheng, Jiao, Zhou, & Shang, 2016). There is an increased effort to use soil spectroscopy at local, regional and global scales (Padarian & McBratney, 2020; Stevens, Nocita, Tóth, Montanarella, & van Wesemael, 2013). Consequently, several initiatives have been launched to compile databases and spectral libraries, which can be used as an operational tool for routinely measuring soil properties. These libraries were established using a standardized spectroscopic measurement of very large numbers of samples, such as the World Soil Spectral Library (Brown et al., 2006), the ICRAF-ISRIC spectral library (Batjes, 2014) and the Global Soil Spectral library (Viscarra Rossel et al., 2016).

This study aims to:

- provide a basic characterization of spectral reflectance curve behaviours of soils in northern Jordan, focusing on soil colour and geochemical components;

- investigate the effect of Fe oxides on the spectral curve behaviour; and
- contribute to the objective of establishing a spectral library of soils in Jordan and to include it in the global spectral library of the world's soil.

Morphological characteristics of the spectra were combined with statistical analysis. Soil reflectance spectra permitted a qualitative and statistical grouping of the soils in terms of spectral reflectance values (SRV) and colour.

2 | MATERIALS AND METHODS

The study area is situated in northern Jordan (longitude 35.90° to 36.29°E; latitude 32.34° to 32.52°N) and covers 693.77 km². The elevation ranges between 1,020 (in the SW) and 500 m a.s.l (in the N and NE). The main soil types

in the area are Chromoxererts, Calcixerollic and Xerochreptic Calciorthids (MOA, 1995). In older classifications, these soils belong to the groups of the Red and Yellow Mediterranean soils (Moormann, 1959) (Figure 1). They cover mainly flat to undulating landscapes. These include the Quaternary plain (fluvial deposits, sand and loess) of the Irbid-Ramtha basin in the northwest, and the dissected limestone plateau of Ajloun in the southwest. Hilly terrain in the central part consists of Tertiary calcareous rocks. Between the hilly terrain and the plain of Irbid, a considerable area is covered by alluvial fans from the limestone plateau. To the east, an undulating to rolling topography and a flat to gently sloping lava plateau are present. According to the long-term records of the average annual rainfall, precipitation falls from more than 600 mm in the west to less than 100 mm in the east. Soil colours change from dark red and brown in the west to lighter colours (more or less yellow) towards the east (Moormann,
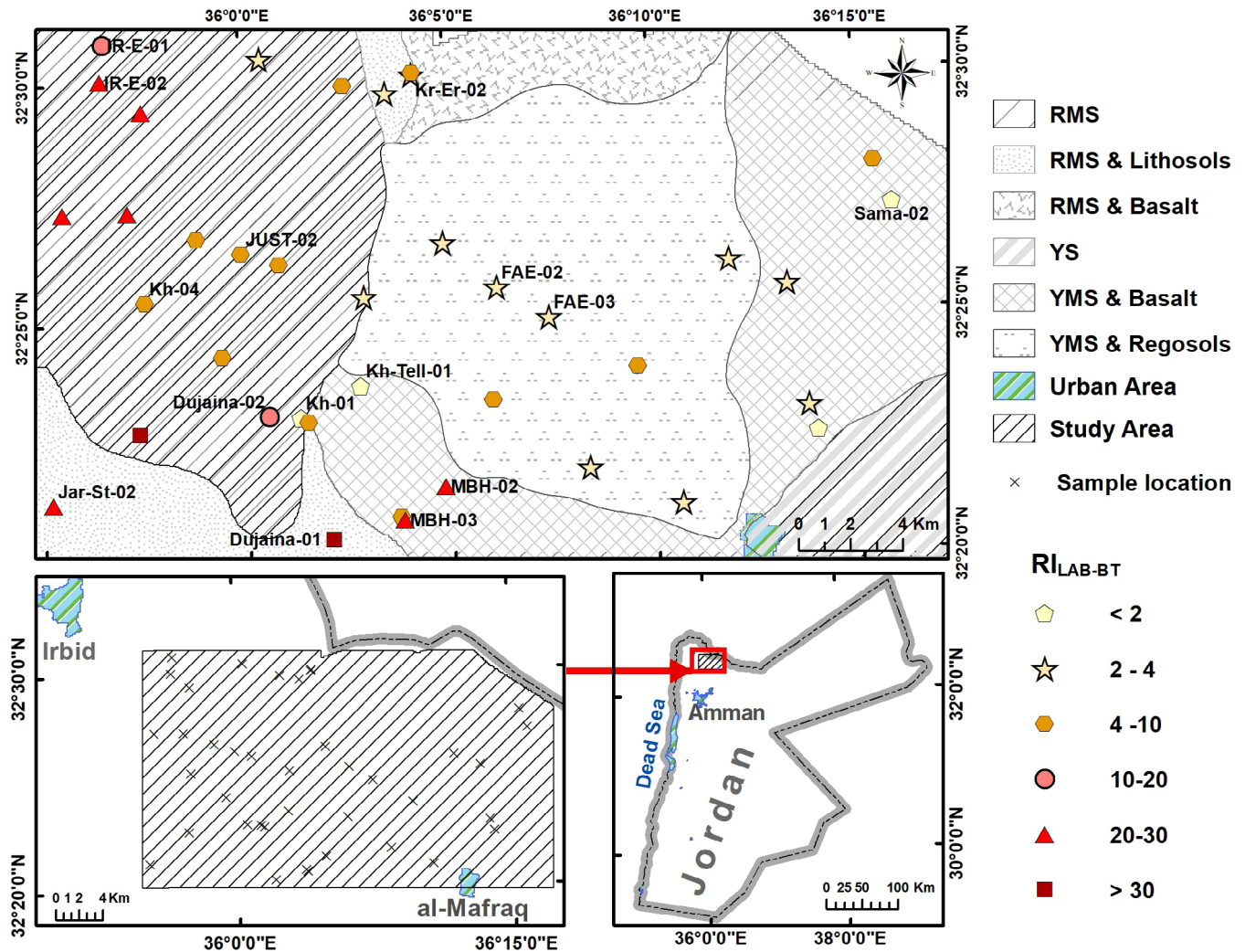

FIGURE 1 Study area, sample locations (labelling names of samples mentioned in text); soil groups from this study according to RI_{LAB-BT}; old USDA soil types referring to colour are given in the background of the map (modified after Moorman, 1959). R= red; M= Mediterranean; S= soils; Y= yellow. RI_{LAB-BT}: redness index based on CIELAB colour system after Barrón and Torrent (1986)

1959; Sahwan, Lucke, Kappas, & Bäumler, 2018). Lucke and Sprafke (2015) suggested that the haematite content increases towards the west, following the current climatic gradient and leading to redder and darker soil colours.

2.1 | Soil sampling

The soil sampling sites were located along the different landscape units as well as on transects of soil colour (40 locations covering yellow to red soil colours; see Moormann, 1959; Lucke & Sprafke, 2015; Sahwan et al., 2018). Every site was georeferenced using a global positioning system (GPS). The samples were taken from a depth of 0–10 cm, mainly on fields used as arable land.

A systematic sample collection with 30-m squares was applied in each location. The samples are from four corners of these squares (labeled A, B, C and D). The collected material (152 samples) was stored in freezer bags. Additional control samples (mixture of soil and quarry dust/aggregates) were taken from a limestone quarry and from the top of the highest archaeological tell in the area (Tell Khanasreh). On this hill, a thin soil cover apparently represents settled dust (Lucke et al., 2019). To minimize the effects of soil moisture and particle size on the spectral measurements, all samples were sieved to ≤2 mm and oven-dried at 40°C for 72 hr. Equal quantities of the samples (A, B, C and D) from each location were mixed in the laboratory. The produced mixtures were used to define the chemical components. A detailed list of sampling locations, Munsell dry colours and general description of the geomorphology is provided in Appendix 1, as well as descriptive statistics of selected chemical parameters of the soil samples in Appendix 2.

2.2 | Spectral measurement and preprocessing

Laboratory soil reflectance spectra were obtained at the Department of Land Surface Dynamics in DLR (German Aerospace Center) using an analytical spectral device (ASD Field Spec® 3 Hi-Res). The ASD measures reflectance in the VIS–NIR and SWIR (0.4–2.5 μm) spectral range, with a spectral resolution of 3 nm in the 0.4–1.0 μm range and of 10–12 nm in the 1.0–2.5 μm range. A high-intensity contact probe (HICP) with a built-in light source (6.5 W halogen lamp) and a measurement surface area equivalent to a 10-mm diameter circle was used to acquire the soil spectra. The HICP was applied to minimize errors associated with stray light. Each sample was placed in a black petri dish and subsequently scanned four times. The sensor was calibrated with a Spectralon panel as white reference once for every sample.

Possible steps in the spectrum were eliminated using the splice correction function of the ASD ViewSpec Pro software. The mean soil reflectance spectra (MSRSs) of each location were calculated from 16 measurements (four samples of each location and four-times repeated measurement). All MSRSs were normalized using the smoothing filter function sgolayfilt in R (Savitzky & Golay, 1964), which reduces high-frequency noise without demeaning the shape of the original spectra (Sellitto, Fernandes, Barrón, & Colombo, 2009). Furthermore, the normalization procedure of continuum removal (CR) was applied to evaluate the absorption features (Clark et al., 2003. This approach has been used successfully in soil science and mineralogy (e.g., Clark et al., 2003; Gomez, Lagacherie, & Coulouma, 2008; Lagacherie, Baret, Feret, Netto, & Robbez-Masson, 2008; Viscarra Rossel, Cattle, Ortega, & Fouad, 2009). In our work, the calculation of CR was achieved using the DISPEC software in ENVI. The spectrum was normalized by setting the hull value to 100% reflection (Clark & Roush, 1984). Two methods can be used to normalize the spectrum: subtraction (additive) or division (multiplicative). The additive technique of CR was applied in our study (Clark et al., 2003).

2.3 | Soil colour and chemical measurements

A ColorLite spectrophotometer sph850 (Katlenburg-Lindau, Germany) was used to measure the soil colours of the oven-dried fine earth. The measuring field of the spectrophotometer has a diameter of 3.5 mm; the light source is D65 and the observer angle 10°. The spectral resolution is 3.5 nm in a range from 400 to 700 nm. The measurement values are the average from two times three replicates with stirring of soil material in between the measurements. The ColorDaTra 1.0.181.5912 software was used to transfer the spectral values and colour parameters into an Excel file, in which the redness index RI_{LAB-BT} of Barrón and Torrent (1986) was calculated. This parameter uses the L* (luminance; black (0), white (100)), a* (intensity of green (<0) or red (>0) component) and b* (intensity of blue (<0) or yellow (>0) component) values of the CIELAB colour space, which is widely used in soil science (Lucke & Sprafke, 2015; Sprafke, 2016; Viscarra Rossel et al., 2009):

$$RI_{LAB-BT} = \frac{a* \left((a*)^2 + (b*)^2 \right)^{0.5} . 10^{10}}{b* . L*^6}. \tag{1}$$

TABLE 1 Selected analytical properties and redness index, $RI_{LAB\text{-}BT}$, after CIELAB according to Barrón and Torrent (1986), of the studied soil samples

Sample	pH_w	C_{org} %	Fe_d mg/g	Fe_t %	Fe_2O_3 %	$CaCO_3$ %	CaO %	$RI_{LAB\text{-}BT}$
Dujaina-01	8.1	0.9	20.4	5.8	15.41	2.82	3.62	48.58
Dujaina-02	8.9	0.8	12	4.5	12.20	15.78	10.15	11.05
FAE-01	8.9	1.4	9.1	4.9	10.16	17.46	14.22	2.6
FAE-02	9.1	1.1	8.8	4.3	9.46	20.07	15.46	2.55
FAE-03	9	1.1	9	4.8	9.64	16.70	13.97	2.9
FAE-N-01	9	0.9	9.1	5.6	9.77	17.39	14.87	2.34
IR-E-01	7.7	0.7	12.2	5	13.22	13.07	8.70	10.87
IR-E-02	9.3	0.7	12.2	4.8	11.90	19.12	12.23	29.55
IR-E-03	8.9	0.9	13.1	5.2	12.77	7.34	6.08	22.27
IR-E-04	9.4	0.8	7.9	4.5	12.17	16.66	10.01	25.7
IR-St-01	9.2	0.7	8.5	4.1	10.68	18.09	11.36	3.73
IR-St-02	9.1	1.6	9.5	3.9	10.68	11.85	8.23	6.58
IR-St-03	9.3	0.8	12	3.6	10.02	26.93	16.54	2.9
Jar-St-01	9	0.8	16.6	5.3	13.58	7.03	5.99	40.52
Jar-St-02	8.8	2.6	17.1	5	13.45	5.33	4.81	21.86
JUST-01	9	1.1	9.5	4.1	10.91	18.40	12.07	4.54
JUST-02	9.2	0.8	10.9	4.4	12.23	13.99	9.37	4.87
JUST-03	8.9	0.8	13.3	6.1	11.78	11.32	10.05	9.84
Kh-01a	8.2	1.4	7.7	2.8	8.06	42.55	22.15	1.9
Kh-02	8.2	0.7	12.8	4.8	12.28	15.20	9.26	4.82
Kh-03	8.2	0.4	11.2	4.9	7.01	17.00	10.34	4.58
Kh-04	8.1	0.5	11.7	4.6	6.63	19.30	11.09	5.72
Kh-05	8.1	0.8	15.15	5.1	7.32	12.90	8.48	29.51
Kh-Tell-01	8.4	2.7	5.6	2.2	3.2	48.00	25.81	1.72
Kr-Ch-01	8.2	1	10.4	4.1	5.87	20.17	11.95	1.75
Kr-Ch-02	9.3	0.4	8	5.9	8.39	34.58	2.30	3.22
Kr-Er-01	8	0.8	8.7	3.8	5.44	20.20	13.40	4.36
Kr-Er-02	8	1.5	10.4	4	5.69	12.24	8.74	3.58
Maf-W-01	8.8	0.9	8.5	4.9	7.03	19.06	17.01	2.18
Maf-W-02	8.2	1.8	9.1	4.5	6.42	21.82	13.98	2.98
MBH-01	8.2	2.1	11.2	5.3	7.54	6.69	7.01	4.16
MBH-02	8.3	1.2	15.9	5.2	7.38	1.15	2.26	21.29
MBH-03	8.8	0.6	13.5	5.9	8.39	15.84	11.93	28.54
MBH-04	8.8	0.8	10.1	3.8	5.47	28.03	17.62	7.56
Quarry	8.6	0.4	4.1	1.1	1.53	78.00	39.18	*
R-SA-01	8.4	1	10.8	4.3	6.17	14.01	9.15	4.08
Sama-01	7.9	0.7	14.4	5.4	7.66	11.18	8.51	6.31
Sama-02	8.3	0.9	10.8	3.8	5.42	24.22	17.36	1.68
Sumaya-01	9.2	1	9.1	3.9	5.62	16.29	10.14	3.23
Sumaya-02	7.8	1.9	9.4	3.8	5.44	8.14	11.75	3.09

L*	a*	b*	RI_LAB-BT	R	G	B	RGB
47.27	10.67	18.64	11.05	139.57	105.00	80.59	

Dujaina-02 (Fe_d 12.0mg/g CaCO_3 16%)

Gr. III

L*	a*	b*	RI_LAB-BT	R	G	B	RGB
62.14	8.95	21.70	1.68	178.79	143.71	111.28	

Sama-02 (Fe_d 10.8mg/g CaCO_3 24%)

Gr. VI

L*	a*	b*	RI_LAB-BT	R	G	B	RGB
39.34	9.08	13.81	29.55	114.53	86.92	70.03	

IR-E-02 (Fe_d 12.2mg/g CaCO_3 19%)

Gr. II

L*	a*	b*	RI_LAB-BT	R	G	B	RGB
58.09	9.02	21.10	2.55	167.43	133.19	102.31	

FAE-02 (Fe_d 8.8mg/g CaCO_3 20%)

Gr. V

L*	a*	b*	RI_LAB-BT	R	G	B	RGB
36.47	9.01	11.54	48.58	106.14	80.25	67.11	

Dujaina-01 (Fe_d 20.4mg/g CaCO_3 3%)

Gr. I

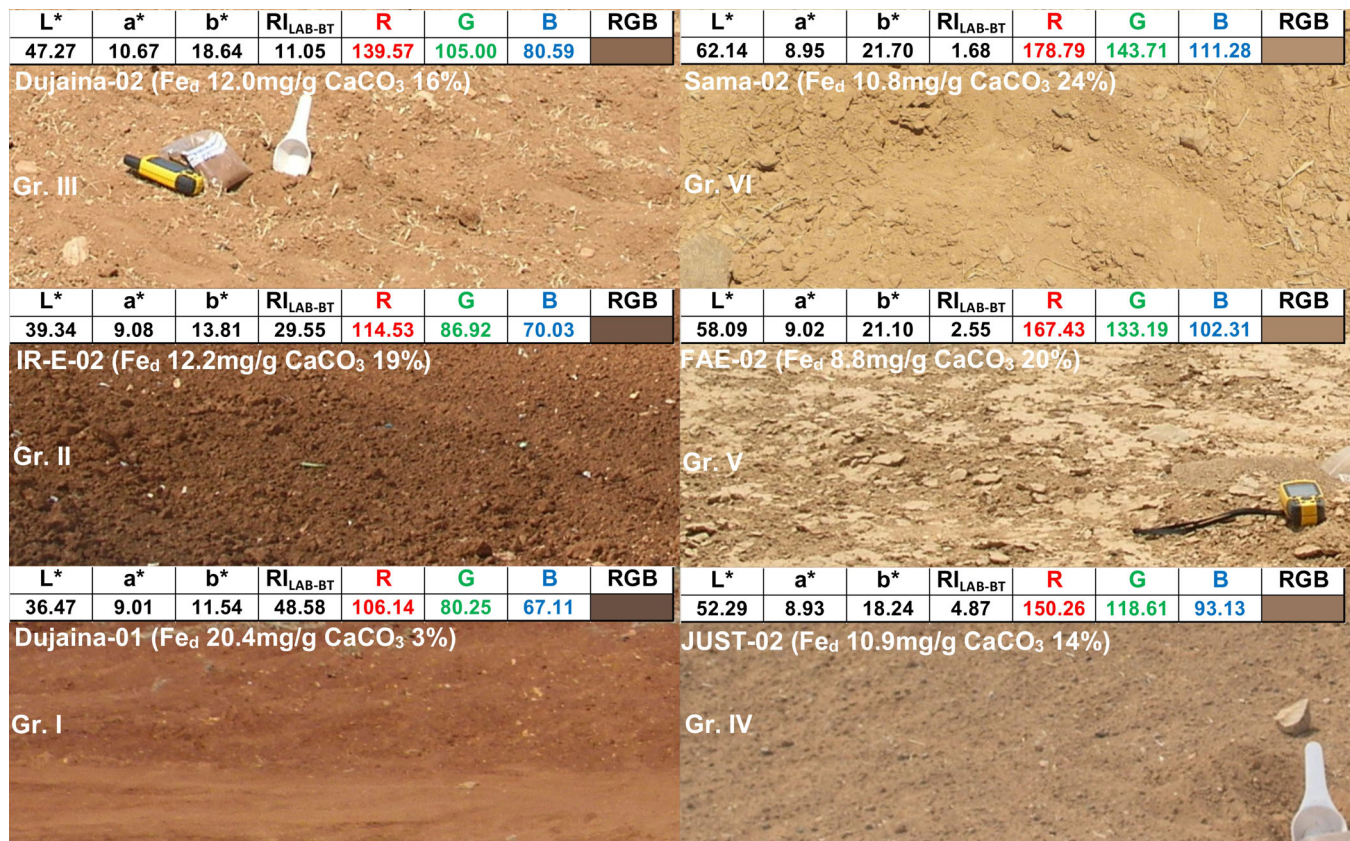| L*	a*	b*	RI_LAB-BT	R	G	B	RGB
52.29	8.93	18.24	4.87	150.26	118.61	93.13	

JUST-02 (Fe_d 10.9mg/g CaCO_3 14%)

Gr. IV

FIGURE 2 Photos and colour data including visualized RGB colours of representative examples for the variation of soil colours in the area

For comparison and general soil description, soil colours were determined with the Munsell Soil Colour chart (Munsell Color Company, 1994) under constant laboratory light by one observer only. This study uses colour measurements of the CIELAB system for statistical and cluster analysis as it is more suitable than the descriptions of Munsell (Barrón & Torrent, 1986; Melville & Atkinson, 1985; Viscarra Rossel et al., 2009). The pH value was determined in distilled water with a glass electrode (pH-meter 530 by WTW, with electrode InLab 423 by Mettler-Toledo) in a soil:water solution of 1:2.5. Contents of soil organic carbon SOC (C_{org}) that is directly related to soil organic matter (SOM) contents and contents of calcium carbonate ($CaCO_3$) were determined using an Elementar vario EL cube C/N-analyser, measuring samples twice before and after ignition for 2 hr at 500°C based on the assumptions that organic matter is ignited and all remaining carbon is inorganic carbon. The free iron oxides, Fe_d (pedogenic oxides), were extracted with sodium dithionite at room temperature according to Holmgren (Schlichting, Blume, & Stahr, 1995). Fe_d quantifies the presence of Fe^{3+} minerals in soils and is an indicator for goethite and haematite (Parfitt & Childs, 1988). For total element analysis and calculation of total iron content (Fe_t), samples were pulverized in an agate ring mill, type Retsch RS 200. Then the loss on ignition was determined by weighing the powder before and after drying for (a) 12 hr at 105°C in a cabinet dryer and (b) 12 hr at 1,030°C in a muffle furnace. Major element oxides such as CaO (used in this study) were measured with an energy-dispersive XRF (Spectro XEPOS plus) at the GeoZentrum Nordbayern (Erlangen, Germany). Precision and accuracy are generally higher than 0.9% (main elements) and 5% (trace elements).

2.4 | Statistical analysis

We applied simple linear regression using the R-function lm (R Core Team, 2018) to examine the relationship between different variables. In particular, we evaluated the performance of reflectance values of MSRSs in all spectral wavelength ranges (SWR) as an independent variable to predict RI_{LAB-BT}, Fe_d and C_{org}. Furthermore, we assessed the relationships between the redness index RI_{LAB-BT} and chemical soil components such as C_{org}, CaO (calculated from total elements measured by XRF) and Fe_d. The linear model was also used to determine the slopes of MSRSs in the ranges 450–600 nm (SCS450) and 600–750 nm (SCS600). A non-linear model (exponential) evaluated the relationship of the coefficients in these two

cases (SCS450 and SCS600) with the RI_{LAB-BT}. To classify the samples according to their L*, a* and b* values and reflectance values, the agglomerative hierarchical cluster analysis with Euclidean distance and complete linkage was applied using the R-function hclust (Maechler, Rousseeuw, Struyf, Hubert, & Hornik, 2019). The results are presented as dendrograms, which were drawn with the R-function as.dendrogram (R Core Team, 2018).

3 | RESULTS

3.1 | Soil chemical and colour properties

The samples represent alkaline soils with pH_w from 7.7 to 9.4. The calcium carbonate contents vary widely between 1 and 48%. Also Fe_d (4.1–20.4 mg/g), as well as the total iron content Fe_t (1.1–6.1%), shows considerable

variation. Most of the soils contain less than 1.9% organic carbon (C_{org}). In the sample from the area of the limestone quarry, the calcium carbonate content is 78%. The RI_{LAB-BT} values range from 1.68 to 48.58 (Table 1) (Figure 2). The high RI_{LAB-BT} of some samples can probably be attributed to high haematite contents (Barrón & Torrent, 1986; Lucke & Sprafke, 2015). Therefore, it seems likely that the soil of light brown or yellow colours with low RI_{LAB-BT} indicates the minor presence of haematite (Table 1 and Figure 2).

3.2 | Spectra of surface soils

The mean soil reflectance spectra MSRSs (Figure 3) have approximately the same behaviour and rather comparable absorption features in the region of hygroscopic water (SWIR: 1400, 1900 nm) and in the region of clay minerals/
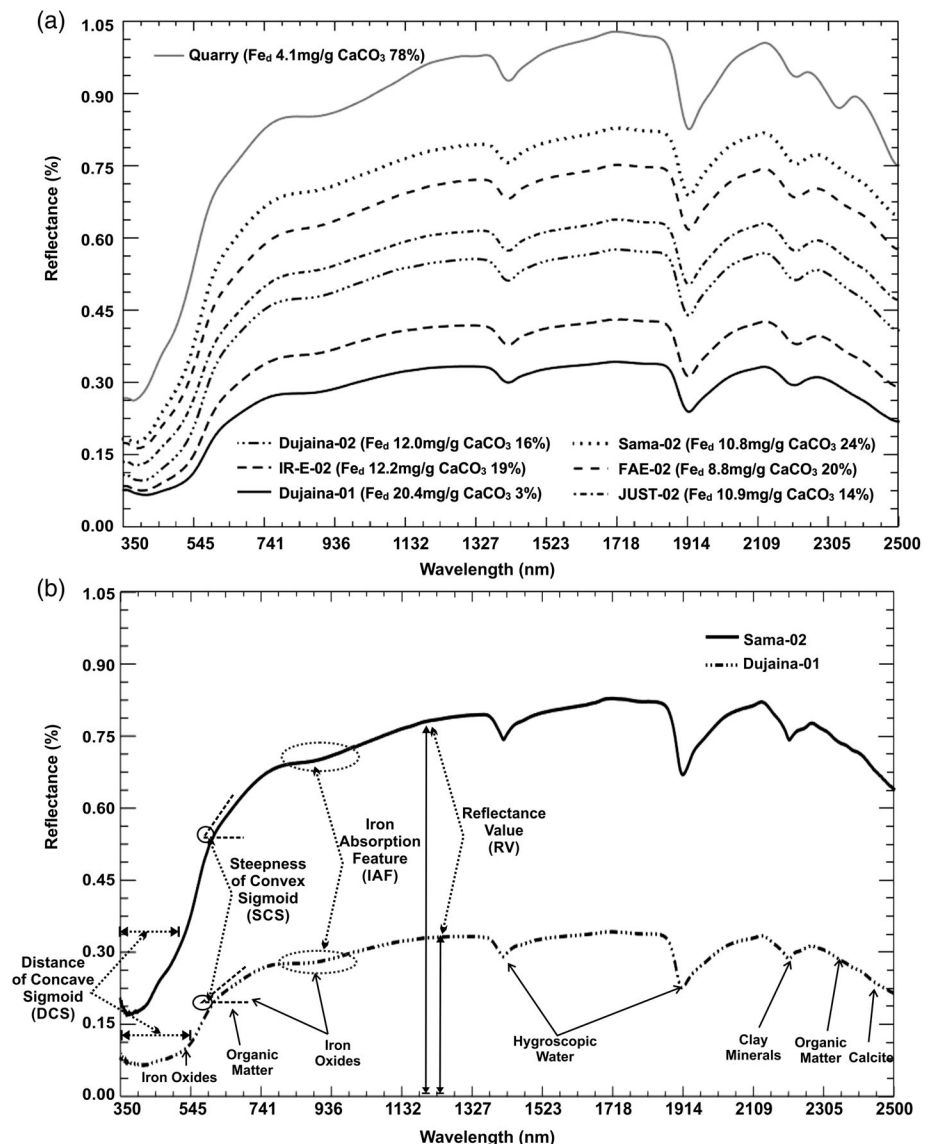

FIGURE 3 (a) Representative spectra of selected soil samples and (b) illustration of morphological conditions of curves

organic matter (SWIR > 2,200 nm) (Baumgardner et al., 1986; Ben-Dor et al., 2008). However, they are characterized by decreasing slope steepness in the VIS range 350–780 nm with sigmoidal form, followed by slight absorption features from 780 to 980 nm (NIR) (Figure 3). Accordingly, all MSRSs represent types of spectral soil curves that are affected by Fe oxides (Bowker, Davis, Myrick, Stacy, & Jones, 1985; Condit, 1970; Escadafal & Huete, 1992; Stoner & Baumgardner, 1981). The effects of Fe oxides on spectra can be illustrated using four morphological distinctions (Demattę, Bellinaso, Romero, & Fongaro, 2014; Poppiel et al., 2018), as in Figure 3:

1 reflectance intensity value (RIV);
2 distance between concave sigmoid and *y*-axis (DCS);
3 steepness of convex sigmoid (SCS); and
4 iron absorption feature (IAF).

Even though the RIV represents a cumulative condition of all soil properties in the entire spectral range, it may show an overall decrease when the Fe content increases, especially if the Fe oxides occur predominantly in the form of haematite (Demattę et al., 2014). In contrast to RIV, the DCS, SCS and IAF elucidate the effects of Fe oxides and SOM in the visible and near-infrared range
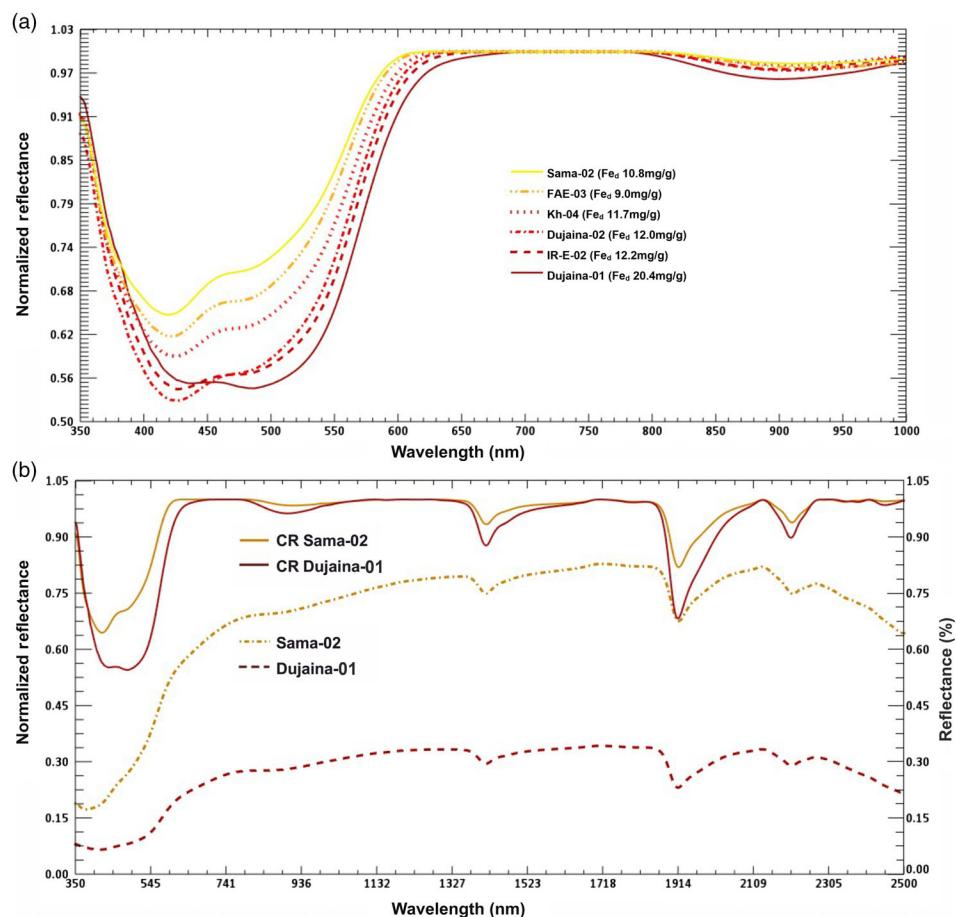

FIGURE 4 (a) Continuum removal (CR) spectra for representative samples illustrate the deepest absorption shiftings in the range (350–1,000 nm). (b) Spectra of Dujaina-01 and Sama-02; the dashed lines show the original spectra and the full lines the CR spectra (350–2,500 nm)

TABLE 2 Parameters of absorption bands in the VIS (visible range) and NIR (near infrared range) of CR (continuum removal) for selective representative samples

Sample	Wavelength (nm)	Depth	Width (nm)	Area	Wavelength (nm)	Depth	Width (nm)	Area
Dujaina-01	479	45.36	192.74	8,743.26	895	3.73	161.57	602.01
IR-E-02	425	45.45	185.59	8,435.68	905	2.40	141.13	338.99
Dujaina-02	425	46.87	178.78	8,379.37	907	2.53	162.83	412.46
Kh-04	424	41.34	175.42	7,251.58	907	1.78	143.61	256.06
FAE-03	425	38.46	168.27	6,472.23	926	2.13	205.73	437.55
Sama-02	424	35.54	163.88	5,823.60	920	1.63	179.80	292.23

FIGURE 5 (a) Representative mean soil reflectance spectra (MSRS) compared with the MSRS of Tell Khanasri (Kh-Tell-01). (b) Summary statistics (calculated in R) of linear correlations SRV (spectral reflectance values) versus Corg and SRV versus Fed
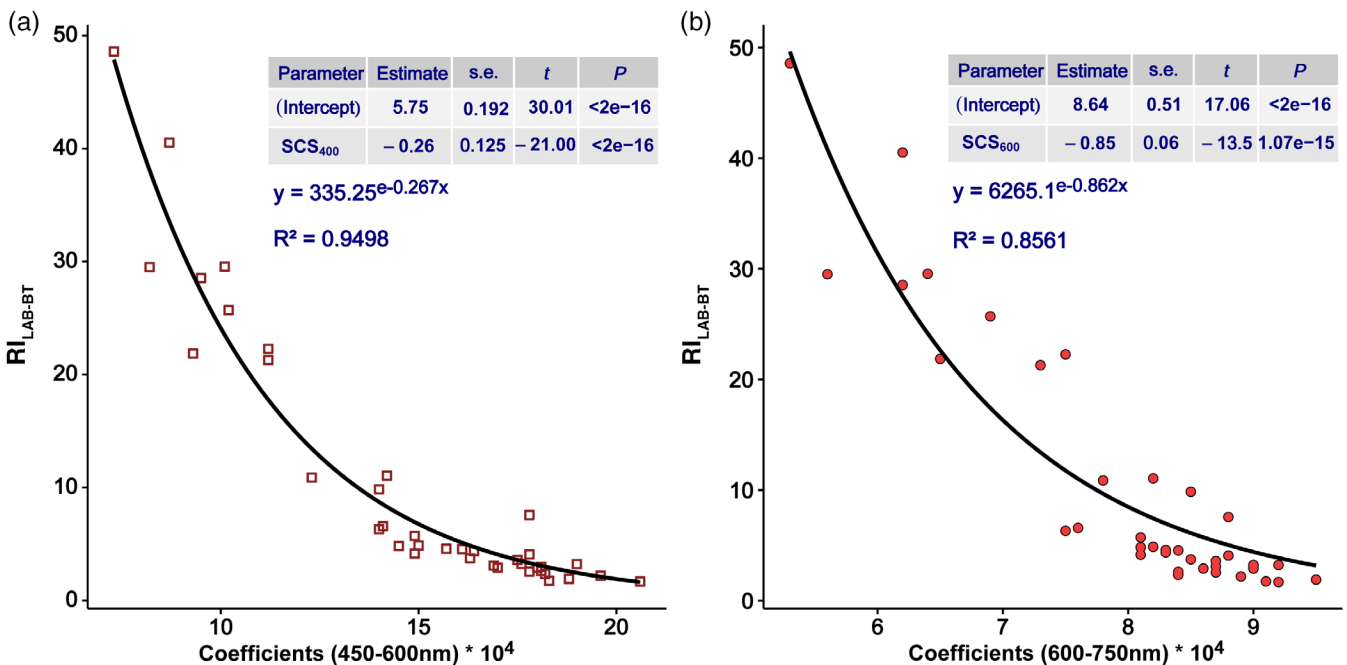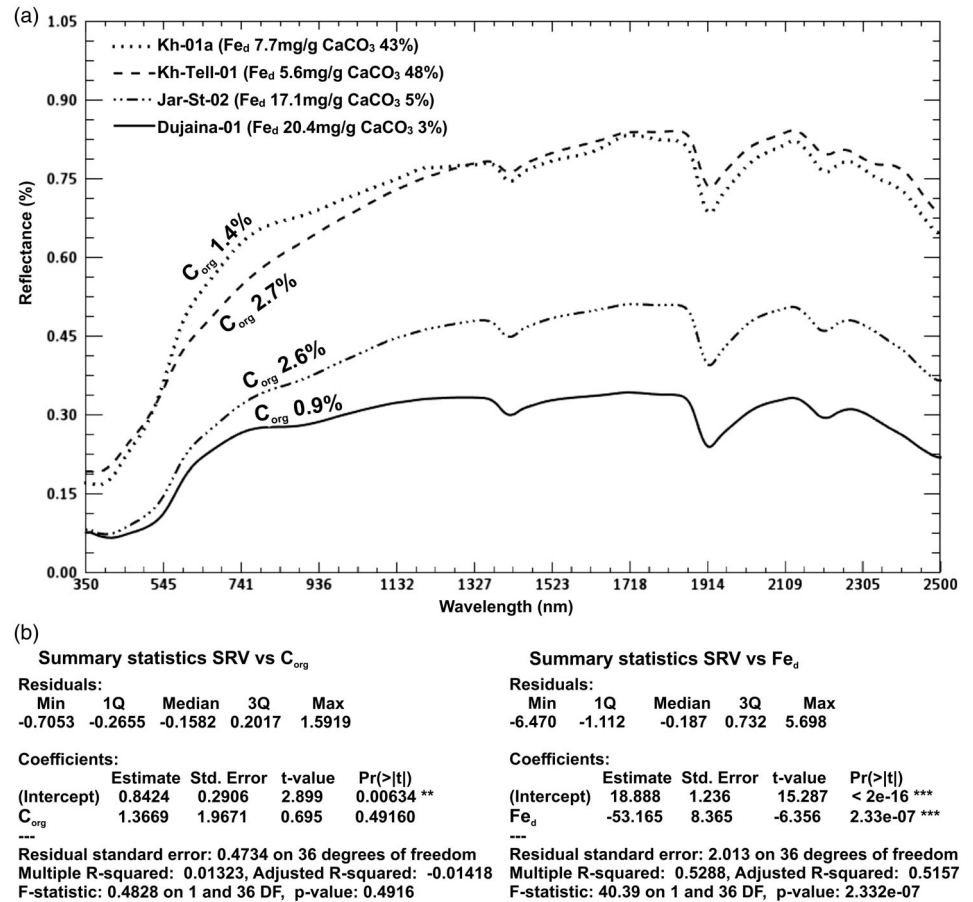

(a)

Kh-01a (Fe_d 7.7mg/g CaCO_3 43%)
Kh-Tell-01 (Fe_d 5.6mg/g CaCO_3 48%)
Jar-St-02 (Fe_d 17.1mg/g CaCO_3 5%)
Dujaina-01 (Fe_d 20.4mg/g CaCO_3 3%)

C_{org} 1.4%
C_{org} 2.7%
C_{org} 2.6%
C_{org} 0.9%

(b)

Summary statistics SRV vs C_{org}

Residuals:

Min	1Q	Median	3Q	Max
-0.7053	-0.2655	-0.1582	0.2017	1.5919

Coefficients:

	Estimate	Std. Error	t-value	Pr(>|t|)
(Intercept)	0.8424	0.2906	2.899	0.00634 **
C_{org}	1.3669	1.9671	0.695	0.49160

Residual standard error: 0.4734 on 36 degrees of freedom
Multiple R-squared: 0.01323, Adjusted R-squared: -0.01418
F-statistic: 0.4828 on 1 and 36 DF, p-value: 0.4916

Summary statistics SRV vs Fe_d

Residuals:

Min	1Q	Median	3Q	Max
-6.470	-1.112	-0.187	0.732	5.698

Coefficients:

	Estimate	Std. Error	t-value	Pr(>|t|)
(Intercept)	18.888	1.236	15.287	< 2e-16 ***
Fe_d	-53.165	8.365	-6.356	2.33e-07 ***

Residual standard error: 2.013 on 36 degrees of freedom
Multiple R-squared: 0.5288, Adjusted R-squared: 0.5157
F-statistic: 40.39 on 1 and 36 DF, p-value: 2.332e-07

(a)

Parameter	Estimate	s.e.	t	P
(Intercept)	5.75	0.192	30.01	<2e-16
SCS_{400}	-0.26	0.125	-21.00	<2e-16

$y = 335.25e^{-0.267x}$

$R^2 = 0.9498$

(b)

Parameter	Estimate	s.e.	t	P
(Intercept)	8.64	0.51	17.06	<2e-16
SCS_{600}	-0.85	0.06	-13.5	1.07e-15

$y = 6265.1e^{-0.862x}$

$R^2 = 0.8561$

FIGURE 6 Exponential correlation (calculated in R) between RI_{LAB-BT} and SCS (slope steepness of sigmoidal form in mean soil reflectance spectra [MSRS]), with tables of regression coefficients (s. e. [standard error], *t*-value, and *p*-value)

(VIS–NIR, 400–1,100 nm). This also depends on the effects of soil moisture and particle size, which are minimized by oven drying and sieving the samples in this study (Escadafal & Huete, 1992; Hoffer, 1978; Hunt, 1980).

The continuum removal (CR) manifests the slight absorption features in the range 780–980 nm. Furthermore, it shows strong absorption features in the range from 350 nm to approximately 700 nm, which was not observable in the original spectra (Figure 4) (Table 2). In these ranges the deepest absorption features show diverse shifts, which can be related to the presence of different Fe minerals (Hunt, 1977; Hunt & Ashley, 1979).

4 | DISCUSSION

4.1 | Effects of chemical components on soil spectra

The soil spectra are from the type of soil affected by Fe oxides (Stoner & Baumgardner, 1981). However, the effect of SOM (or SOC) can mask the effects of Fe oxides and cause a smoothing of their absorption features (Baumgardner et al., 1986; Ben-Dor, 2002; Viscarra Rossel

TABLE 3 The spectral ranges with R^2 values (Fe_d content - RVs) higher than average

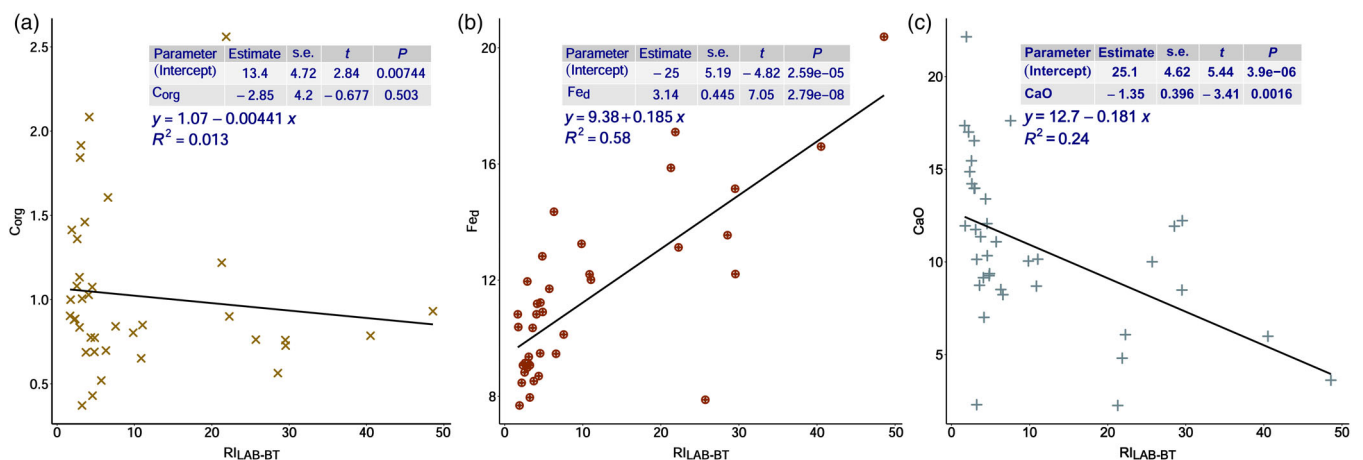| SWR (nm)	R^2	SWR (nm)	R^2	SWR (nm)	R^2
478–510	0.54	560–579	0.57	734–794	0.60
511–538	0.55	580–616	0.58	795–903	0.59
539–559	0.56	617–733	0.59	904–1,040	0.58

RVs, reflectance values; SWR, spectral wavelength ranges.

et al., 2016). This masking is noticeable solely in the sample from the summit of Tell Khanasri (Kh-Tell-01, C_{org} 2.7% and Fe_d 5.6 mg/g) and in the sample Jar-St-02 (C_{org} 2.6% and Fe_d 17.1 mg/g) (Figure 5). In contrast to these two samples, the contents of C_{org} are less than 2.1% in all other samples (Table 1). According to Baumgardner, Kristof, Johannsen, and Zachary (1969), the masking effects become less effective if the SOM contents drop below 2.0%. The statistical analysis using linear models leads to the same result. In this context, the correlations of reflectance values of MSRSs in all spectral wavelength ranges (SWR) with Fe_d and C_{org} were investigated. The coefficient of determination (R^2) was fairly low (lower than 0.03, $p > .5$) in the case of C_{org} (R^2 average value = 0.013). In contrast, it was considerable in the case of Fe_d, for which the average value of R^2 was 0.53.

Concerning the above-mentioned conditions, the effects of Fe oxides on MSRS properties dominate, whereas the effects of SOC are generally negligible (Figures 3 and 5). In this regard, the RIV of MSRSs increases from dark red-brown soils to yellow soils. The samples of low RIV have a high content of Fe as well as a low content of $CaCO_3$ (or CaO) and vice-versa (Figure 3 and Table 1). Moreover, the samples with high RIV are closer to the RIV of the sample from the limestone quarry and show considerable absorption in the range of the calcite effect (Sama-02 in Figure 3). Some samples (e.g., IR-E-02 and Dujaina-02) have diverse RIV, despite comparable contents of Fe and $CaCO_3$ (Figure 3). This could be the result of increasing haematite contents in comparison to goethite and calcite (Cañasveras Sánchez, Barrón, Del Campillo, & Viscarra Rossel, 2012; Curcio, Ciraolo, D'Asaro, & Minacapilli, 2013; Fernandes, Barrón, Torrent, & Fontes, 2004). It is consistent with the trend of RI_{LAB-BT} values, which are high in IR-E-02 and low in Dujaina-02 (Table 1).

FIGURE 7 Correlations of RI_{LAB-BT} with Corg, Fed and CaO, with tables of regression coefficients calculated in R (s. e. [standard error], t-value and p-value)

TABLE 4　Comparison of the cluster ranking sorted by redness index, RI_{LAB-BT}, according to Barrón and Torrent (1986)

| Sample | Group | Clustering | | RI_{LAB-BT} | Sample | Group | Clustering | | RI_{LAB-BT} |
		Spectral	Colour				Spectral	Colour	
Dujaina-01	I	I	I	48.58	Kh-03	IV	IV	III	4.58
Jar-St-01	I	I	I	40.52	JUST-01	IV	IV	V	4.54
Kh-05	I	I	II	29.51	IR-St-01	IV	IV	V	3.73
MBH-03	I	I	II	28.54	Sumaya-02	IV	IV	V	3.09
Jar-St-02	II	II	II	21.86	IR-St-03	V	V	V	2.90
IR-E-02	II	II	II	29.55	Sumaya-01	V	V	V	3.23
IR-E-04	II	II	II	25.70	Kr-Er-01	V	V	IV	4.36
MBH-02	II	II	II	21.29	Kr-Er-02	V	V	V	3.58
IR-E-03	II	II	II	22.27	FAE-03	V	V	V	2.90
IR-E-01	III	III	III	10.87	R-SA-01	V	V	V	4.08
JUST-03	III	III	III	9.84	Maf-W-02	V	V	V	2.98
Dujaina-02	III	III	III	11.05	FAE-02	V	V	V	2.55
Sama-01	III	III	IV	6.31	FAE-01	V	V	V	2.60
Kh-02	IV	IV	III	4.82	Kr-Ch-02	V	V	V	3.22
Kh-04	IV	IV	III	5.72	FAE-N-01	V	V	V	2.34
IR-St-02	IV	III	IV	6.58	Maf-W-01	VI	VI	VI	2.18
MBH-01	IV	IV	IV	4.16	Kr-Ch-01	VI	VI	VI	1.75
MBH-04	IV	IV	IV	7.56	Kh-01a	VI	VI	VI	1.90
JUST-02	IV	IV	IV	4.87	Sama-02	VI	VI	VI	1.68

In general, soils rich in $CaCO_3$ and relatively poor in Fe show higher reflectance than soil with less or negligible $CaCO_3$ content, or with high Fe content (Gaur, Pandey, & Goyal, 2016). The morphological conditions DCS, SCS and IAF show the following trends: the DCS decreases from red soils to yellow soils, and the steepness (SCS) changes from relatively low (red soils) to high (yellow soils). Taking into consideration the negligible effects of SOC, the low SCS is related to an increased proportion of haematite in comparison to goethite (Demattę et al., 2014; Poppiel et al., 2018). In our study, this finding is considerable because of the relationship between the morphological condition SCS and RI_{LAB-BT}, which can be used as an indicator of the proportion of haematite/goethite (Barrón & Torrent, 1986). This relation was statistically highlighted using the linear correlation between RI_{LAB-BT} and SCS in the ranges of 450–600 nm (SCS_{450}) and 600–750 nm (SCS_{600}). To facilitate this correlation, the slopes of MSRSs in the ranges SCS_{450} and SCS_{600} were extracted using linear regression. The coefficients of these two cases (SCS_{450} and SCS_{600}) show strong exponential correlations with the RI_{LAB-BT} (Figure 6). The R-squared values were 0.95 ($p < 0.001$) and 0.86 ($p < 0.001$), respectively. Furthermore, the SCS_{450} and SCS_{600} show a considerable linear correlation with Fe_d ($R^2 = 0.60$, $p < 0.001$). In contrast,

there is no significant relationship with other chemical components (e.g., with C_{org}: $R^2 = 0.004$, $p > .5$).

According to the statistical analysis of linear correlation between reflectance values of MSRSs in all spectral wavelength ranges (SWR) and Fe_d, the highest R^2 value (0.60, $p < 0.001$) is recorded in the spectral range of 734–794 nm. Table 3 shows that the coefficients of determination (R^2) are higher than average ($R^2 = 0.54$) in several SWRs, which correspond to the absorption features of Fe oxides in the form of haematite or goethite (Grove, Hook, & Paylor, 1992; Hunt & Ashley, 1979; Morris et al. 1985). According to Grove et al. (1992), for example, haematite shows absorption maxima at 535 nm and goethite at 503 nm.

In this regard, the continuum removal (CR) curves evaluate the possible presence of haematite or goethite. For example, the deepest absorption demonstrates a shift from 479 nm (Dujaina-01) to 424 nm (Sama-02) in the visible range (Figure 4). Further shifting occurs in the range of near infrared from 895 nm (Dujaina-01) to 920 nm (Sama-02). These two shifts point to a decrease of haematite and increase of goethite from Dujaina-01 to Sama-02 (Hunt, 1977; Hunt and Ashley, 1979; Morris et al., 1985; Vilas, Jarvis, & Gaffey, 1994). As a general trend, there is a relatively high presence of haematite in
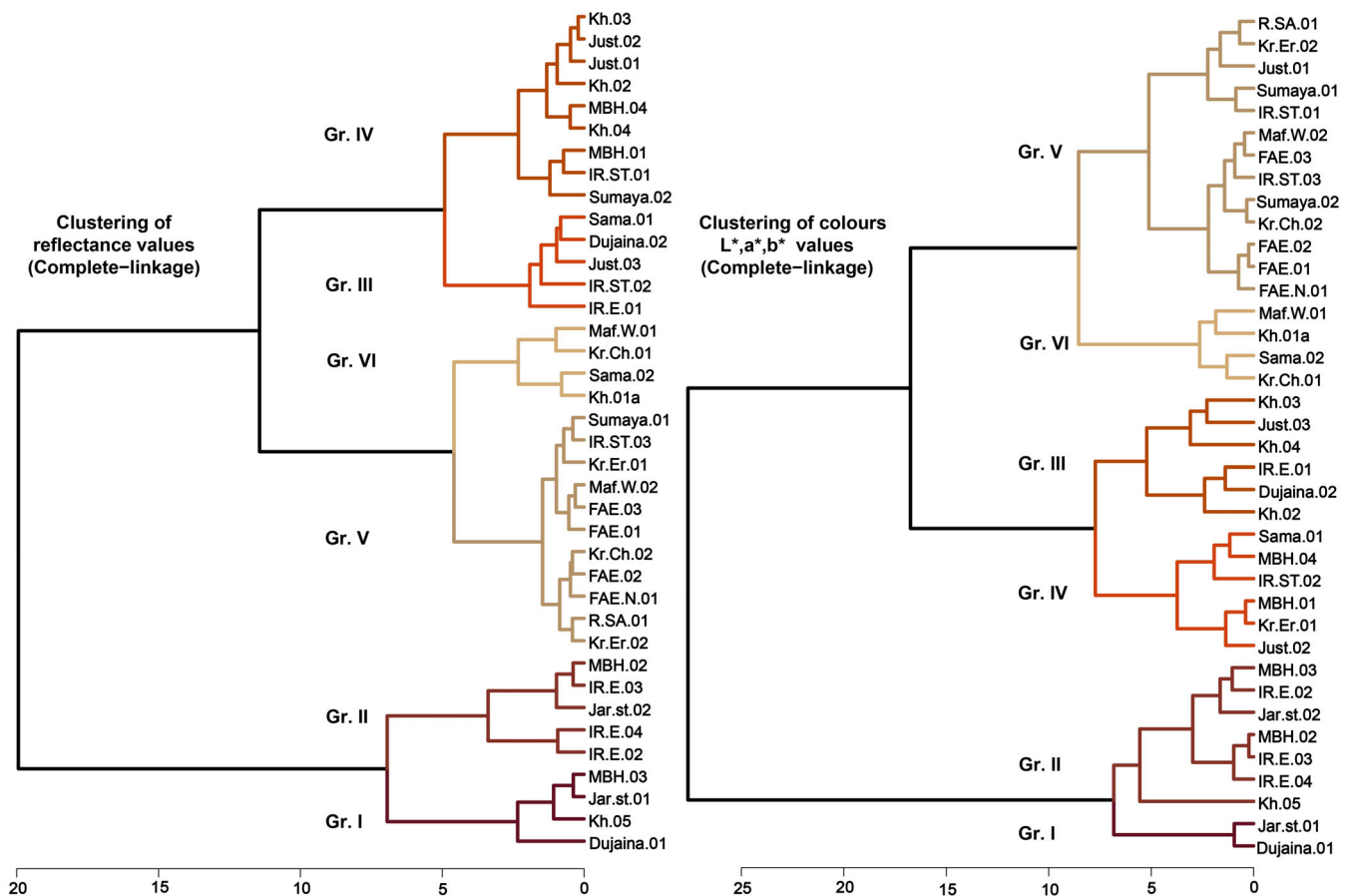
FIGURE 8 Statistical clustering of spectral reflectance values and soil colour values (L*, a* and b*) using complete linkage in R Software' Gr., Group

samples from western parts of the study area and a relatively low presence of haematite in samples from eastern parts. This result is consistent with studies on surface soil weathering intensity in the context of the current climatic gradients in this area (Lucke & Sprafke, 2015; Sahwan et al., 2018).

4.2 | Correlation of soil colours with chemical components

Considering the relatively low contents of C_{org} (SOC), the Fe oxides (probably haematite/goethite) are the dominant pigmenting agents. This suggests that the redness index RI_{LAB-BT} is an adequate indicator of haematite and goethite contents in soils, as proposed by Barrón and Torrent (1986). The relationships between RI_{LAB-BT} and chemical soil components such as C_{org}, CaO (calculated using XRF) and Fe_d were insignificant, significant and highly significant, respectively (Figure 7). This indicates a negligible effect of SOC on the colours of the samples. The low correlation with the CaO content indicates that calcium carbonate does not play a decisive role. In

contrast, the considerable correlation with Fe_d ($R^2 = 0.58$, $p < 0.001$) reflects the effect of Fe oxides on soil colour.

4.3 | Soil grouping

Depending on the morphological conditions, the mean soil reflectance spectra MSRSs were arranged qualitatively in six groups: Group I to Group VI (Table 4). Figure 3 illustrates representative reflectance curves of these groups. A hierarchical cluster analysis of all MSRSs reflectance values and soil colour values (L*, a* and b*) was conducted (Table 2 and Figure 8). This qualitative grouping and clustering of spectral values categorized all samples to matching groups with the exception of some outliers, which showed strongly divergent properties (Table 4).

The ranking corresponds to the decrease of haematite effects and increase of $CaCO_3$ effects from the first group (Group I) to the sixth group (Group VI). It more or less reflects a categorization of RI_{LAB-BT} values in the following groups: $RI_{LAB-BT} > 30$, 30–20, 20–10, 10–4, 4–2 and

$RI_{LAB-BT} < 2$. This matching can be established through the high linear correlation ($R^2 = 0.82$, $p < 0.001$) of RI_{LAB-BT} with all spectral values of MSRSs in all SWRs.

Compared with the map of Moormann (1959), the samples of Group I, Group II and Group III are mostly located in the areas of Red Mediterranean Soils, and Red Mediterranean Soils and Lithosols (see Figure 1). A few samples, such as MBH-03 and MBH-02 (Group II), are located in the area of Yellow Mediterranean Soils and Basalt. These samples show high effects of haematite on the spectral curves and colours. Another deviation in classification compared to the map of Moormann is the case of sample Kr-Er-02 in the transitional zone between Red Mediterranean Soils and Yellow Mediterranean Soils. This area is the geomorphologic boundary between the hilly terrain of Tertiary calcareous rocks in the central part and the level area to the west, where water surface flow and limestone debris deposition processes are active. Due to these local geomorphic influences, this sample has relatively low haematite and high $CaCO_3$ contents. In the clustering of this study, this sample is classified in Group V, which has a low value of RI_{LAB-BT} and shows minor effects of Fe oxides. Such local variation cannot be detected on large-scale maps. Their mapping and monitoring need a precise evaluation of remotely sensed satellite data. However, such studies require a site-specific spectral library, which can be used as ground truthing data to facilitate the use of current and future multispectral and hyperspectral satellite data. In this regard, spectra from spectral libraries facilitate a highly precise classification of remotely sensed satellite data, in order to evaluate the spatial distribution of red soils in the area (Sahwan et al., 2018).

5 | CONCLUSIONS

This study combined the evaluation of laboratory reflectance spectra of surface soils in northern Jordan with systematic ground observations and laboratory measurements of soil properties. A significant amount of surface soil samples that represent an initial database of a soil spectral library of Jordan was collected. The extracted representative MSRSs of this study confirm that spectra of soils of similar landscape setting in northern Jordan depend on the iron oxides. This refers mainly to the pigmenting effects of haematite and goethite, which seem closely connected with the intensity of *in-situ* pedogenesis of surface soils in the study area, mirroring the current climatic gradients. To a more limited degree, contents of calcium carbonate play a role, too, in particular with regard to soil brightness. Our study discriminated morphological conditions of spectral curves that permit

distinguishing between these spectra. Statistically, the study demonstrated a clear relationship between spectra, chemical components and colour characteristics of the soils. It shows that the significant contrast between the spectra results from Fe oxide effects connected to the proportion of hematite and goethite, which are the dominant soil colour agents.

Even though the spectra show partial similarity, they can be classified into six spectral groups, which highly coincide with soil colour groups. Consequently, our results can be used as a basis to assess soil colour with multispectral or hyperspectral data and thereby analyse the chemical and mineralogical properties of soils in Jordan. Such studies are essential to avoid unreliable classification of remote sensing data because of behaviour similarity of spectral curves. In summary, spectral characteristics can provide an alternative method to the traditional and highly expensive methods for assessing soil properties in Jordan. However, further studies on the prediction of constituents such as iron, organic matter and clay fraction should be conducted in order to enlarge the available data and their robustness, which will facilitate soil surveys and management practices in Jordan.

CONFLICTS OF INTEREST
None.

DATA AVAILABILITY STATEMENT
I herewith confirm that the data that support the findings of this study are available from the corresponding author upon reasonable request.

ORCID
Wahib Sahwan [ID] https://orcid.org/0000-0002-6503-5525
Tobias Sprafke [ID] https://orcid.org/0000-0003-1198-4482

REFERENCES
Al-Qudah, B. (2001). Soils of Jordan. In Zdruli, P., Steduto, P., Lacirignola, L., and Montanarella, L. (eds). Soil resources of Southern and Eastern Mediterranean countries (pp. 127–141). Bari, Italy: CIHEAM-IAMB.

Barrón, V., & Torrent, J. (1986). Use of the Kubelka—Munk theory to study the influence of iron oxides on soil colour. *Journal of Soil Science*, 37(4), 499–510.

Batjes, N. H. (2014). *A globally distributed soil spectral library visible near infrared diffuse reflectance spectra*. World Agroforestry Centre (ICRAF). https://library.wur.nl/WebQuery/isricpubs/451105.

Baumgardner, M. F., Kristof, S., Johannsen, C. J., & Zachary, A. (1969). Effects of organic matter on the multispectral properties of soils. In *Proceedings of the Indiana Academy of science* (Vol. 79, pp. 413–422). West Lafayette, IN:). Purdue University.

Baumgardner, M. F., Silva, L. F., Biehl, L. L., & Stoner, E. R. (1986). Reflectance properties of soils. In *Advances in agronomy* (Vol. 38, pp. 1–44). New York, NY: Academic Press.

Ben-Dor, E. (2002). Quantitative remote sensing of soil properties. *Advances in Agronomy*, 75, 173–244.

Ben-Dor, E., Taylor, R. G., Hill, J., Demattê, J. A. M., Whiting, M. L., Chabrillat, S., & Sommer, S. (2008). Imaging spectrometry for soil applications. *Advances in Agronomy*, 97, 321–392.

Bowers, S. A., & Hanks, R. J. (1965). Reflection of radiant energy from soils. *Soil Science*, 100(2), 130–138. Retrieved from https://journals.lww.com/soilsci/Fulltext/1965/08000/REFLECTION_OF_RADIANT_ENERGY_FROM_SOILS.9.aspx

Bowker, D. E., Davis, R. E., Myrick, D. L., Stacy, K., & Jones, W. T. (1985). Spectral reflectances of natural targets for use in remote sensing studies, NASA Langley Research Center, No. Preference Publication-1139, Hampton, VA.

Brown, D. J., Shepherd, K. D., Walsh, M. G., Dewayne Mays, M., & Reinsch, T. G. (2006). Global soil characterization with VNIR diffuse reflectance spectroscopy. *Geoderma*, 132(3–4), 273–290. https://doi.org/10.1016/j.geoderma.2005.04.025

Camargo, L. A., Júnior, J. M., Barrón, V., Alleoni, L. R. F., Barbosa, R. S., & Pereira, G. T. (2015). Mapping of clay, iron oxide and adsorbed phosphate in Oxisols using diffuse reflectance spectroscopy. *Geoderma*, 251, 124–132.

Cañasveras SánchezJ. C., Barrón V., Del Campillo M. C., Viscarra Rossel R. A. (2012). Reflectance spectroscopy: a tool for predicting soil properties related to the incidence of Fe chlorosis. *Spanish Journal of Agricultural Research*, 10(4), 1133. http://dx.doi.org/10.5424/sjar/2012104-681-11.

Chabrillat, S., Ben-Dor, E., Cierniewski, J., Gomez, C., Schmid, T., & van Wesemael, B. (2019). Imaging spectroscopy for soil mapping and monitoring. *Surveys in Geophysics*, 40(3), 361–399.

Clark, R. N., & Roush, T. L. (1984). Reflectance spectroscopy: Quantitative analysis techniques for remote sensing applications. *Journal of Geophysical Research*, 89(B7), 6329–6340.

Clark, R. N., Swayze, G. A., Livo, K. E., Kokaly, R. F., Sutley, S. J., Dalton, J. B., McDougal, R. R., Gent, C. A. (2003). Imaging spectroscopy: Earth and planetary remote sensing with the USGS Tetracorder and expert systems. *Journal of Geophysical Research: Planets*, 108, (E12), p. 5-1–p. 5-44. http://dx.doi.org/10.1029/2002je001847.

Condit, H. R. (1970). The spectral reflectance of American soils. *Photogrammetric Engineering Remote Sensing*, 36, 955–966.

Curcio, D., Ciraolo, G., D'Asaro, F., & Minacapilli, M. (2013). Prediction of soil texture distributions using VNIR-SWIR reflectance spectroscopy. *Procedia Environmental Sciences*, 19, 494–503.

Demattê, J. A. M., Bellinaso, H., Romero, D. J., & Fongaro, C. T. (2014). Morphological interpretation of reflectance Spectrum

(MIRS) using libraries looking. *Science in Agriculture*, 71(6), 509–520.

Escadafal, R., Girard, M. C., & Courault, D. (1989). Munsell soil color and soil reflectance in the visible spectral bands of Landsat MSS and TM data. *Remote Sensing of Environment*, 27 (1), 37–46.

Escadafal, R., & Huete, A. R. (1992). Soil optical properties and environmental applications of remote sensing. *International Archives of Photogrammetry and Remote Sensing*, 29, 709–715.

Fernandes, R. B. A., Barrón, V., Torrent, J., & Fontes, M. P. F. (2004). Quantificação de óxidos de ferro de Latossolos brasileiros por espectroscopia de refletância difusa. *Revista Brasileira de Ciência Do Solo*, 28(2), 245–257.

Gaur, M. K., Pandey, C. B., & Goyal, R. K. (Eds.). (2016). *Remote sensing for natural resources monitoring & management*. Jodhpur, India: Scientific Publishers. isbn:9789386102720.

Gomez, C., Lagacherie, P., & Coulouma, G. (2008). Continuum removal versus PLSR method for clay and calcium carbonate content estimation from laboratory and airborne hyperspectral measurements. *Geoderma*, 148(2), 141–148.

Grove, C. I., Hook, S. J., & Paylor III, E. D. (1992). *Laboratory reflectance spectra of 160 minerals, 0.4 to 2.5 micrometers*. Pasadena, CA: NASA Jet Propulsion Laboratory, 92–2.

Hill, J., & Schütt, B. (2000). Mapping complex patterns of erosion and stability in dry Mediterranean ecosystems. *Remote Sensing of Environment*, 74, 557–569.

Hoffer, R. M. (1978). Biological and physical considerations in applying computer-aided analysis techniques to remote sensor data. In P. H. Swain & S. M. Davis (Eds.), *Remote sensing: The quantitative approach* (pp. 227–289). New York, NY: McGraw-Hill.

Huete, A. R. (1996). Extension of soil spectra to the satellite: Atmosphere, geometric, and sensor considerations. *Photo Interprétation (Paris)*, 34(2), 101–118.

Huete, A. R., & Escadafal, R. (1991). Assessment of biophysical soil properties through spectral decomposition techniques. *Remote Sensing of Environment*, 35(2–3), 149–159.

Hunt, G. R., & Ashley, R. P. (1979). Spectra of altered rocks in the visible and near infrared. *Economic Geology*, 74(7), 1613–1629.

Hunt, G. R. (1977). Spectral signatures of particulate minerals in the visible and near infrared. *Geophysics*, 42(3), 501–513.

Hunt, G. R. (1980). Electromagnetic radiation: The communication link in remote sensing. In B. S. Siegal & A. R. Gillesppie (Eds.), *Remote sensing in geology* (pp. 5–45). New York, NY: Wiley.

Irons, J. R., Weismiller, R. A., & Peterson, G. W. (1989). Soil reflectance. In G. Asrar (Ed.), *Theory and applications of optical remote sensing* (pp. 66–106). New York, NY: J. Wiley & Sons..

Lagacherie, P., Baret, F., Feret, J. B., Netto, J. M., & Robbez-Masson, J. M. (2008). Estimation of soil clay and calcium carbonate using laboratory, field and airborne hyperspectral measurements. *Remote Sensing of Environment*, 112(3), 825–835.

Lucke, B. (2008). Demise of the Decapolis. In *Past and present desertification in the context of soil development, land use, and climate*. Saarbrücken, Germany: OmniScriptum. isbn: 978-3639006131.

Lucke, B. (2017). *Landscape transformations in the context of soil development, land use, and climate: A comparison of marrginal areas in Jordan, Mexico, and Germany*. Stuttgart, Germany:

Gebrüder Bornträger. Relief Boden Paläoklima 26. ISBN 978-3443090265.

Lucke, B., Kemnitz, H., & Bäumler, R. (2012). Evidence for iso-volumetric replacement in terrae Rossae of Jordan. *Boletín de la Sociedad Geológica Mexicana*, *64*(1), 21–35.

Lucke, B., Kemnitz, H., Bäumler, R., & Schmidt, M. (2014). Red Mediterranean soils in Jordan: New insights in their origin, genesis, and role as environmental archives. *Catena*, *112*, 4–24.

Lucke, B., Nikolskii, I., Schmidt, M., Bäumler, R., Nowaczyk, N., & al-Saad, Z. (2008). The impact of drought in the light of changing soil properties. In J. Sánchez (Ed.), *Droughts: Causes, effects, and predictions* (pp. 69–102). New York, NY: Nova Science Publishers.

Lucke, B., Roskin, J., Vanselow, K. A., Bruins, H. J., Abu-Jaber, N., Deckers, K., ... Bäumler, R. (2019). Character, rates, and environmental significance of Holocene Dust accumulation in archaeological Hilltop Ruins in the southern Levant. *Geosciences*, *9*(4), 1–60. https://doi.org/10.3390/geosciences9040190

Lucke, B., Schmidt, M., Al-Saad, Z., Bens, O., & Hüttl, R. F. (2005). The abandonment of the Decapolis region in northern Jordan – Forced by environmental change? *Quaternary International*, *135*, 65–81.

Lucke, B., & Sprafke, T. (2015). Correlation of soil color, redness ratings, and weathering indices of terrae Calcis along a precipitation gradient in northern Jordan. In *Lucke, B., Bäumler, R., Schmidt, M. (eds.) Soils and sediments as archives of environmental change. Geoarchaeology and landscape change in the subtropics and tropics* (pp. 53–68). Erlangen:). Fränkische Geographische Gesellschaft.

Lucke, B., Ziadat, F., & Taimeh, A. (2013). The soils of Jordan. In A. Myriam (Ed.), *Atlas of Jordan: History, Territories and Society*. Atlas Al Urdunn, Al-Tarikh, Al-Ardh, Al-Mujtama. Beyrouth, Lebanon: IFPO.

Maechler, M., Rousseeuw, P., Struyf, A., Hubert, M., & Hornik, K. (2019). Cluster analysis basics and extensions. R Package Version 2.1.0. https://cran.r-project.org/web/packages/cluster/cluster.pdf.

Melville, M. D., & Atkinson, G. (1985). Soil colour: Its measurement and its designation in models of uniform colour space. *Journal of Soil Science*, *36*(4), 495–512.

MOA, Ministry of Agriculture. (1995). *The soils of Jordan*. Report of the National Soil Map and Land Use Project undertaken by Ministry of Agriculture, Huntings Technical Services Ltd and European Commission volume 2: Main report. MOA, Amman, Jordan.

Moormann, F. R. (1959). Report to the Government of Jordan on the Soils of East Jordan: Food and Agriculture Organization of the United Nations FAO (Expanded Technical Assistance Program No. 1132). FAO, Rome.

Morris, R. V., Lauer H. V., Lawson C. A., Gibson E. K., Nace G. A., Stewart C. (1985). Spectral and other physicochemical properties of submicron powders of hematite (α-Fe2O3), maghemite (γ-Fe2O3), magnetite (Fe3O4), goethite (α-FeOOH), and lepidocrocite (γ-FeOOH). *Journal of Geophysical Research*, *90*, (B4), 3126. http://dx.doi.org/10.1029/jb090ib04p03126.

Munsell Color Company. (1994). *Munsell soil color charts* (Rev. ed.). New Windsor, NY: Macbeth Division of Kollmorgen Instruments Corporation.

Nocita, M., Stevens, A., van Wesemael, B., Aitkenhead, M., Bachmann, M., Barthès, B., ... Wetterlind, J. (2015). Soil spectroscopy: An alternative to wet chemistry for soil monitoring. In D. L. Sparks (Ed.), *Advances in agronomy* (Vol. 132, pp. 139–159). Waltham, MA: Academic Press. https://doi.org/10.1016/bs.agron.2015.02.002

NSM and LUP, 1993. Hashemite Kingdom of Jordan, Ministry of Agriculture, Hunting Technical Services Ltd, Soil Survey and Land Research Centre. The soils of Jordan. Level 1, Reconnaissance Soil Survey, Vol. 2, Main Report. Amman, National Soil Map and Land Use Project.

Ogen, Y., Zaluda, J., Francos, N., Goldshleger, N., & Ben-Dor, E. (2019). Cluster-based spectral models for a robust assessment of soil properties. *Geoderma*, *340*, 175–184. https://doi.org/10.1016/j.geoderma.2019.01.022

Padarian, J., & McBratney, A. B. (2020). New model for intra- and inter-institutional soil data sharing. *The Soil*, *6*(1), 89–94. https://doi.org/10.5194/soil-6-89-2020

Parfitt, R. L., & Childs, C. W. (1988). Estimation of forms of Fe and Al - a review, and analysis of contrasting soils by dissolution and Mossbauer methods. *Soil Research*, *26*(1), 121. http://dx.doi.org/10.1071/sr9880121.

Poppiel, R. R., Lacerda, M. P. C., de Oliveira Junior, M. P., Demattê, J. A. M., Romero, D. J., Sato, M. V., ... Cassol, L. F. M. (2018). Surface spectroscopy of Oxisols, Entisols and Inceptisol and relationships with selected soil properties. *Revista Brasileira de Ciência Do Solo*, *42*, 1–26. https://doi.org/10.1590/18069657rbcs20160519

R Core Team. (2018). *R: A language and environment for statistical computing*. Vienna, Austria: R Foundation for Statistical Computing. Retrieved from https://www.R-project.org/

Sahwan, W., Lucke, B., Kappas, M., & Bäumler, R. (2018). Assessing the spatial variability of soil surface colors in northern Jordan using satellite data from Landsat-8 and Sentinel-2. *European Journal of Remote Sensing*, *51*(1), 850–862. https://doi.org/10.1080/22797254.2018.1502624

Savitzky, A., & Golay, M. J. E. (1964). Smoothing and differentiation of data by simplified least squares procedures. *Analytical Chemistry*, *36*(8), 1627–1639. https://doi.org/10.1021/ac60214a047

Schmidt, M., Lucke, B., Bäumler, R., al-Saad, Z., al-Qudah, B., & Hutcheon, A. (2006). The Decapolis region (northern Jordan) as historical example of desertification? Evidence from soil development and distribution. *Quaternary International*, *151*, 74–86.

Schlichting, E., Blume, H. P., & Stahr, K. (1995). *Soils practical. Wissenschafts-Verlag Blackwell, Berlin, Germany*, (p. 295).

Sellitto, V. M., Fernandes, R. B. A., Barrón, V., & Colombo, C. (2009). Comparing two different spectroscopic techniques for the characterization of soil iron oxides: Diffuse versus bi-directional reflectance. *Geoderma*, *149*(1–2), 2–9. https://doi.org/10.1016/j.geoderma.2008.11.020

Sprafke, T. (2016): *Löss in Niederösterreich - Archiv quartärer Klima- und Landschaftsveränderungen* (dissertation). Julius-Maximilians-Universität, Würzburg; Würzburg University Press. https://opus.bibliothek.uni-wuerzburg.de/files/12778/978-3-95826-039-9_Sprafke_Tobias_OPUS_12778.pdf.

Stevens, A., Nocita, M., Tóth, G., Montanarella, L., & van Wesemael, B. (2013). Prediction of soil organic carbon at the European scale by visible and near infrared reflectance spectroscopy. *PLoS One*, *8*(6), e66409. https://doi.org/10.1371/journal.pone.0066409

Stoner, E. R., & Baumgardner, M. F. (1981). Characteristic variations in reflectance of surface soils (remote sensing). With assistance of FAO of the UN. *Soil Science Society of America Journal*, *45*(6), 1161–1165.

United States Department of Agriculture (USDA) (1938). Soils and men. In *Yearbook of agriculture*. Washington, DC: Government Printing Office..

Vilas, F., Jarvis, K. S., & Gaffey, M. J. (1994). Iron alteration minerals in the visible and near-infrared spectra of low-albedo asteroids. *Icarus*, *109*(2), 274–283. https://doi.org/10.1006/icar.1994.1093

Viscarra Rossel, R. A., Behrens, T., Ben-Dor, E., Brown, D. J., Demattê, J. A. M., Shepherd, K. D., … Ji, W. (2016). A global spectral library to characterize the world's soil. *Earth-Science Reviews*, *155*, 198–230. https://doi.org/10.1016/j.earscirev.2016.01.012

Viscarra Rossel, R. A., Cattle, S. R., Ortega, A., & Fouad, Y. (2009). In situ measurements of soil colour, mineral composition and clay content by Vis–NIR spectroscopy. *Geoderma*, *150*(3–4), 253–266. https://doi.org/10.1016/j.geoderma.2009.01.025

Viscarra Rossel, R. A., Rizzo, R., Demattê, J. A. M., & Behrens, T. (2010). Spatial modeling of a soil fertility index using visible-near-infrared spectra and terrain attributes. *Soil Science Society of America Journal*, *74*(4), 1293–1300. https://doi.org/10.2136/sssaj2009.0130

Viscarra Rossel, R. A., Walvoort, D. J. J., McBratney, A. B., Janik, L. J., & Skjemstad, J. O. (2006). Visible, near infrared, mid infrared or combined diffuse reflectance spectroscopy for simultaneous assessment of various soil properties. *Geoderma*, *131*(1–2), 59–75. https://doi.org/10.1016/j.geoderma.2005.03.007

Viscarra Rossel, R. A., & Webster, R. (2011). Discrimination of Australian soil horizons and classes from their visible-near infrared spectra. *European Journal of Soil Science*, *62*(4), 637–647. https://doi.org/10.1111/j.1365-2389.2011.01356.x

Zheng, G., Jiao, C., Zhou, S., & Shang, G. (2016). Analysis of soil chronosequence studies using reflectance spectroscopy. *International Journal of Remote Sensing*, *37*(8), 1881–1901. https://doi.org/10.1080/01431161.2016.1163751

APPENDIX A: Sampling locations, Munsell dry colours and general description of the geomorphology

Sample	N°	E°	Munsell dry	General description
Dujaina-01	32.34068	36.03388	5YR, 4/4 reddish brown	Flat area/moderately dissected limestone plateau/Ajloun
Dujaina-02	32.38378	36.00913	7.5YR, 6/4 light brown	Toeslope/moderately dissected limestone plateau/Ajloun
FAE-01	32.42422	36.04855	7.5YR, 6/4 light brown	Gentle to flat slope/undulating topography/tertiary calcareous
FAE-02	32.42652	36.10294	7.5YR, 6/4 light brown	Bottom of Wadi/undulating topography/tertiary calcareous
FAE-03	32.41564	36.12399	7.5YR, 7/3 pink	Toeslope/undulating topography on tertiary calcareous
FAE-N-01	32.44226	36.08156	7.5YR, 6/3 light brown	Flat field/undulating topography/tertiary calcareous
IR-E-01	32.51388	35.94467	7.5YR, 5/4 brown	Flat field/undulating plain/quaternary fluviatile
IR-E-02	32.50102	35.94321	5YR, 5/4 reddish brown	Flat field/undulating plain/quaternary fluviatile
IR-E-03	32.49005	35.95956	5YR, 5/4 reddish brown	Flat field/undulating plain/quaternary fluviatile
IR-E-04	32.45509	35.95311	7.5YR, 7/4 pink	Flat field/undulating plain/quaternary fluviatile
IR-St-01	32.50776	36.00835	7.5YR, 7/6 reddish yellow	Flat field/extensive alluvial fans derived from limestone
IR-St-02	32.49767	36.04232	10YR,8/2 very pale brown	Flat field/extensive alluvial fans derived from limestone
IR-St-03	32.49463	36.05936	5YR,6/3 light reddish brown	Toeslope/extensive alluvial fans derived from limestone
Jar-St-01	32.37846	35.95591	2.5YR, 4/4 reddish brown	Toeslope/moderately dissected limestone plateau/Ajloun
Jar-St-02	32.35477	35.91987	5YR, 5/4 reddish brown	Slope-shoulder/moderately dissected limestone plateau/Ajloun
JUST-01	32.44573	35.98099	7.5YR, 7/4 pink	Toeslope/extensive alluvial fans derived from limestone
JUST-02	32.44030	35.99910	5YR, 5/3 reddish brown	Wadi-bottom/alluvial fans/dissected limestone
JUST-03	32.43633	36.01449	7.5YR, 6/3 light brown	Wadi-bottom/alluvial fans/dissected limestone
Kh-01a	32.38304	36.02180	7.5YR, 6/6 reddish yellow	Slope-shoulder /extensive alluvial fans derived from limestone
Kh-02	32.38304	36.02180	7.5YR, 5/6 strong brown	Back slope/extensive alluvial fans derived from limestone
Kh-03	32.40475	35.99036	7.5YR, 5/6 strong brown	Flat field/moderately dissected limestone plateau/Ajloun
Kh-04	32.42413	35.95922	7.5YR, 5/8 strong brown	Flat field/undulating plain/quaternary fluviatile
Kh-05	32.45600	35.92658	7.5YR, 4/6 strong brown	Flat field/undulating plain/quaternary fluviatile
Kh-Tell-01	32.39361	36.04655	5YR, 6/2 pinkish grey	Summit of tell/dissected limestone
Kr-Ch-01	32.37464	36.23282	7.5YR, 6/6 reddish yellow	Flat field/flat lava plateau
Kr-Ch-02	32.38330	36.22923	7.5 YR, 7/4 pink	Flat field/flat lava plateau
Kr-Er-01	32.50165	36.07062	7.5YR, 6/6 reddish yellow	Flat field/toeslope/undulating topography/tertiary calcareous
Kr-Er-02	32.50083	36.07042	7.5YR, 6/6 reddish yellow	Footslope/undulating topography/tertiary calcareous
Maf-W-01	32.35020	36.17689	7.5YR, 7/3 pink	Wadi-bottom/undulating topography/tertiary calcareous
Maf-W-02	32.36328	36.13917	10YR,7/3 very pale brown	Footslope/finely dissected uplands/Belqa limestone
MBH-01	32.38775	36.10049	7.5YR, 6/3 light brown	Backslope/undulating topography/tertiary calcareous
MBH-02	32.35795	36.08011	5YR, 5/4 reddish brown	Footslope/finely dissected uplands/Belqa limestone
MBH-03	32.34679	36.06308	2.5YR, 4/4 reddish brown	Toeslope/moderately dissected limestone plateau/Ajloun
MBH-04	32.34803	36.06180	7.5YR, 6/6 reddish yellow	Footslope/moderately dissected limestone plateau/Ajloun

(Continues)

Sample	N°	E°	Munsell dry	General description
Quarry	32.38305	36.02881	5YR, 8/2 pinkish white	Undulating topography/tertiary calcareous
R-SA-01	32.39806	36.15991	7.5YR, 6/6 reddish yellow	Footslope/undulating topography/tertiary calcareous
Sama-01	32.46728	36.25824	7.5YR, 5/6 strong brown	Toeslope/bottom of Wadi/flat lava plateau
Sama-02	32.45308	36.26526	7.5YR, 6/6 reddish yellow	Flat field/flat lava plateau
Sumaya-01	32.43428	36.19799	10YR,6/4 light yellowish brown	Footslope/undulating topography/tertiary calcareous
Sumaya-02	32.42552	36.22151	7.5YR, 7/4 brown	Toeslope/flat lava plateau

APPENDIX B: Descriptive statistics of selected chemical parameters of the soil samples

Chemical characters	pH	$C_{org}\%$	Fe_d (mg/g)	$Fe_2O_3\%$	$Fe_t\%$	$CaCO_3\%$	CaO%	Ca%
Min	7.73	0.37	6.00	4.06	2.84	1.15	2.26	1.60
Max	9.43	2.56	20.38	8.77	6.14	42.55	22.15	15.73
Mean	8.63	1.02	10.69	6.65	4.65	16.31	10.85	7.70
Standard deviation	0.50	0.46	3.09	1.04	0.73	7.99	4.30	3.05